Beam Theory and Modeling at US HIF-VNL

Hong Qin

Plasma Physics Laboratory

Princeton University

2004 US-Japan Workshop on Heavy Ion Fusion

June 10-12, 2004

Princeton, NJ

Beam theory studies at the US Heavy Ion Fusion Virtual National Laboratory are focused on the dynamics and instabilities of high intensity beams, and beam-plasma interaction.

- Instability study.
- Beam compression and final focusing.
- Chamber transport.

Nonlinear Kinetic Stability Theorem

- An important feature of intense beam propagation is the existence of a stability theorem based on the nonlinear Vlasov-Maxwell equations.*

- For a long, one-component coasting beam in the smooth-focusing approximation, the stability theorem expressed in the beam frame ($\beta_b = 0$ and $\gamma_b = 1$) states that any equilibrium distribution function $f_b^0(H)$ that satisfies

$$\frac{\partial}{\partial H} f_b^0(H) \leq 0$$

  is nonlinearly stable to perturbations with arbitrary polarization.

- Here, $H = (p_r^2 + p_\theta^2 + p_z^2)/2m_b + m_b\omega_f^2 r^2/2 + e_b\phi^0(r)$ is the single-particle Hamiltonian in the beam frame, and $\phi^0(r)$ is the electrostatic potential determined self-consistently from Poisson's equation.

- A necessary condition for instability is that the beam distribution function have some nonthermal feature such as an inverted population in phase space, or a strong energy anisotropy, or that the beam have directed kinetic energy relative to background charge components.

*R. C. Davidson, Phys. Rev. Lett. **81**, 991 (1998).

Collective Instabilities in Intense Charged Particle Beams

One-Component Beams

- Electrostatic Harris instability ($T_{\|b}/T_{\perp b} < 1$)
- Electromagnetic Weibel instability ($T_{\|b}/T_{\perp b} < 1$)

Propagation Through Background Electrons

- Electron-ion two-stream (Electron Cloud) instability

Propagation Through Background Plasma

- Resistive hose instability
- Multispecies Weibel instability
- Multispecies two-stream instability

Harris Instability in Intense One-Component Beams

- Electrostatic Harris instability* can play an important role in multispecies plasmas with temperature anisotropy $T_{\|j} < T_{\perp j}$.
- Harris instability is inherently three-dimensional and involves a coupling of the longitudinal and transverse particle dynamics.
- Harris-like instability† also exists in intense one-component beams provided the anisotropy is sufficiently large ($T_{\|b}/T_{\perp b} \ll 1$) and the beam intensity is sufficiently large.

*E. G. Harris, Phys. Rev. Lett. **2**, 34 (1959).

†I. Haber, et al., Phys. Plasmas **6**, 2254 (1999).

Weibel Instability in Intense One-Component Beams

- The electromagnetic Weibel instability* can play an important role in multispecies anisotropic plasmas and beam-plasma systems.

- However, the Weibel instability is not likely to play an important role in one-component nonneutral beams:
  - Constraints imposed by finite transverse geometry.
  - Electrostatic Harris instability has a much larger growth rate in the region where the Weibel instability exists.

*E. S. Weibel, Phys. Rev. Lett. **2**, 83 (1959).

Weibel Instability in Intense One-Component Beams

Assume axisymmetric perturbations ($\partial/\partial\theta = 0$) and transverse electromagnetic fields with polarization

$$\delta\mathbf{E}^T = \delta E_\theta \hat{\mathbf{e}}_\theta \ , \quad \delta\mathbf{B}^T = \delta B_r \hat{\mathbf{e}}_r + \delta B_z \hat{\mathbf{e}}_z$$

Analysis of the linearized Vlasov-Maxwell equations leads to an infinite dimension matrix dispersion equation*

$$\det\{D_{n,m}(\omega)\} = 0$$

which is valid for arbitrary normalized beam intensity

$$s_b = \frac{\widehat{\omega}_{pb}^2}{2\gamma_b^2\omega_f^2}$$

and temperature anisotropy $T_{\|b}/T_{\perp b}$. Here, $\widehat{\omega}_{pb} = (4\pi\widehat{n}_b e_b^2/\gamma_b m_b)^{1/2}$ is the ion plasma frequency.

*E. A. Startsev and R. C. Davidson, Phys. Plasmas **10**, 4829 (2003).

Weibel Instability in Intense One-Component Beams

In the limit $T_{\|b}/T_{\perp b} \rightarrow 0$, the maximum growth rate of the Weibel instability is

$$(Im\omega)_{\max} = 0.85\widehat{\omega}_{pb}\frac{v_{\perp b}^{th}}{c}$$

for $k_z^2 r_b^2 \gg 1$.

Detailed numerical analysis of matrix dispersion relation equation for finite $T_{\|b}$ shows that the Weibel instability is completely stabilized whenever $T_{\|b}$ exceeds the small threshold value $T_{\|b}^{th}$ defined by

$$\frac{T_{\|b}^{th}}{T_{\perp b}} = 0.2\frac{r_b^2\widehat{\omega}_{pb}^2}{c^2} \ll 1$$

Electron-Ion Two-Stream (Electron Cloud) Instability

- A background population of electrons can result when energetic beam ions strike the chamber wall or ionize background gas atoms.

- Relative streaming motion of beam ions through the background electrons provides the free energy to drive the classical two-stream instability, appropriately modified to include the effects of dc space charge, relativistic kinematics, transverse beam geometry, etc.

- Experimental evidence for two-stream instability in proton machines such as the Proton Storage Ring (PSR) experiment at Los Alamos National Laboratory.

Electron-Ion Two-Stream (Electron Cloud) Instability

- Instability is three-dimensional in nature, with strongest growth exhibited by dipole-mode perturbations with azimuthal mode number $m = 1$. This is a common feature of experiments, analytical theory, and numerical simulations.

- 3D nonlinear delta-f simulations by Qin, et al., using the BEST code, have investigated detailed properties of this instability for a wide range of system parameters. Simulations use a smooth focusing model in which the electrons are confined in the transverse plane by the (excess) space charge of the beam ions.

- Detailed analytical investigations of linear stability properties have also been carried out for arbitrary multipole perturbations about a Kapchinskij-Vladimirskij (KV) distribution with step-function density profile.

Electron-Ion Two-Stream (Electron Cloud) Instability

As a simple example, consider dipole-mode perturbations about a KV distribution. Assume cold beam ions with axial velocity V_b propagate through a stationary electron background ($V_e = 0$).

Dispersion Relation

$$[(\omega - k_z V_b)^2 - \omega_b^2][\omega^2 - \omega_e^2] = \omega_c^4 \ ,$$

Definitions

$$\begin{aligned}
\omega_c^4 &= \frac{1}{4} f \left(1 - \frac{r_b^2}{r_w^2}\right)^2 \frac{\gamma_b m_b}{Z_b m_e} \widehat{\omega}_{pb}^4 \\
\omega_b^2 &= \omega_f^2 + \frac{1}{2} \widehat{\omega}_{pb}^2 \left(f - \frac{1}{\gamma_b^2} \frac{r_b^2}{r_w^2}\right) \\
\omega_e^2 &= \frac{1}{2} \frac{\gamma_b m_b}{Z_b m_e} \widehat{\omega}_{pb}^2 \left(1 - f \frac{r_b^2}{r_w^2}\right)
\end{aligned}$$

where

$$f = \text{fractional charge neutralization}$$

$$\widehat{\omega}_{pb} = \left(\frac{4\pi \widehat{n}_b Z_b^2 e_b^2}{\gamma_b m_b}\right)^{1/2} = \text{ion plasma frequency}$$

Electron-Ion Two-Stream (Electron Cloud) Instability

Growth Rate Reduction Mechanisms

- Axial momentum spread in the beam ions.
- Proximity of a conducting wall.
- Reduction in fractional charge neutralization.
- Rounded beam density profiles
  - Spread in transverse oscillation frequency.

Outline

- Self-similar symmetry if required for focusing the entire beam pulse.
- Longitudinal Dynamics.
  - Self-similar solutions for un-neutralized beams.
  - Self-similar solutions for neutralized beams.
  - Pulse shaping
- Transverse Dynamics and Final Focus.
  - Non-periodic lattice and adiabatically-matched beams.
  - Time-dependent lattice for deviation from self-similar symmetry.

Need Self-Similar Symmetry To Focus the Entire Beam Pulse

⇨ a, b, λ, ε_x, and ε_y for different Z are generated by the same solution through a one-parameter group transformation admitted by the envelope equations

$$\begin{pmatrix} a\left[s, Z(\delta=0)\right] \\ b\left[s, Z(\delta=0)\right] \\ \lambda\left[s, Z(\delta=0)\right] \\ \varepsilon_x\left[s, Z(\delta=0)\right] \\ \varepsilon_y\left[s, Z(\delta=0)\right] \end{pmatrix} \longrightarrow \begin{pmatrix} a\left[s, Z(\delta)\right] \\ b\left[s, Z(\delta)\right] \\ \lambda\left[s, Z(\delta)\right] \\ \varepsilon_x\left[s, Z(\delta)\right] \\ \varepsilon_y\left[s, Z(\delta)\right] \end{pmatrix} .$$

⇨ It is easy to check that the following scaling group is a symmetry group of the envelope equations.

$$\begin{pmatrix} a\left[s, Z(\delta)\right] \\ b\left[s, Z(\delta)\right] \\ \lambda\left[s, Z(\delta)\right] \\ \varepsilon_x\left[s, Z(\delta)\right] \\ \varepsilon_y\left[s, Z(\delta)\right] \end{pmatrix} = \begin{pmatrix} \delta a\left[s, Z(\delta=0)\right] \\ \delta b\left[s, Z(\delta=0)\right] \\ \delta^2\lambda\left[s, Z(\delta=0)\right] \\ \delta^2\varepsilon_x\left[s, Z(\delta=0)\right] \\ \delta^2\varepsilon_y\left[s, Z(\delta=0)\right] \end{pmatrix}$$

Lie Group Symmetry Analysis

- The systematic method for finding similarity solutions (group-invariant solutions) for PDEs is the Lie group symmetry analysis.
- Two types of point symmetries can be used.
  - **Classical point symmetry**, which transfers a solution of the PDEs into another solution.
  - **Non-classical point symmetry**, under which a solution is invariant.
- The symmetry groups of both types are determined by the corresponding infinitesimal generators.
  - Classical point symmetry: linear and algorithmically solvable dertmining equations. Infinitesimal generators form a Lie algebra.
  - Non-classical point symmetry: nonlinear and non-algorithmically-solvable dertmining equations. No infinitesimal Lie algebra.
- Once point symmtries are found, similarity solutions can be derived straightforwardly.

Longitudinal Dynamics – 1D fluid model

- In the beam frame:

$$\begin{aligned}
\frac{\partial \lambda}{\partial t} + \frac{\partial}{\partial z}(\lambda u_z) &= 0 \ \text{(continuity)}, \\
\frac{\partial u_z}{\partial t} + u_z \frac{\partial u_z}{\partial z} + \frac{e^2 g}{m\gamma^5}\frac{\partial \lambda}{\partial z} + \frac{\kappa_z z}{m\gamma^3} + \frac{r_b^2}{m\gamma^3 \lambda}\frac{\partial p_z}{\partial z} &= 0 \ \text{(momentum)}, \\
\frac{\partial p_z}{\partial t} + u_z \frac{\partial p_z}{\partial z} + 3 p_z \frac{\partial u_z}{\partial z} &= 0 \ \text{(energy)}.
\end{aligned}$$

- Nonlinear hyperbolic PDE system
- The energy equation is equivalent to

$$\frac{d}{dt}\left(\frac{p_z}{\lambda^3}\right) = 0.$$

Self-Similar Drift Compression for Neutralized Beams

⇨ Drift compression for neutralized beams modelled by the 1D Vlasov eq.

$$\frac{\partial f}{\partial t} + v_z \frac{\partial f}{\partial z} = 0 \; .$$

⇨ The general solution is a function of two trivial invariants,

$$f(t, z, v_z) = f(0, z - v_z t, v_z) \; .$$

⇨ A class of self-similar drift compression solutions can be more easily constructed using Courant-Snyder invariant

$$\begin{aligned} \chi &= \frac{z^2}{z_b^2(t)} + \frac{z_b^2(t)}{z_{b0}^2 v_{T0}^2}\left[v_z - z_b'(t)\frac{z}{z_b(t)}\right]^2 , \\ \frac{d^2 z_b(t)}{dt^2} &= \frac{z_{b0}^2 v_{T0}^2}{z_b^2(t)} \; . \\ z_b^2(t) &= (z_{bo} + z_{b0}' t)^2 + v_{T0}^2 t^2 \; , \end{aligned}$$

where $z_{b0}' = (dz_b/dt)_{t=0}$ and v_{T0} is an effective thermal speed.

Density Inversion Theorem

- For a given self-similar line density profile, the corresponding distribution function is

$$f(\chi) = -\frac{1}{\pi}\frac{\lambda_b(t) z_b(t)}{z_{b0} v_{T0}} \int_\chi^\infty \frac{\partial h(Z^2)}{\partial Z^2} \frac{dZ^2}{\sqrt{Z^2 - \chi}} \, .$$

- For the family of self-similar line density profiles

$$\lambda(t,z) = \lambda_b(t) h(Z^2) = \begin{cases} \lambda_b(t)(1-Z^2)^n, & Z \le 1, \\ 0, & Z > 1 \, . \end{cases}$$

$$f(\chi) = \begin{cases} -\frac{1}{\sqrt{\pi}}\frac{\lambda_b(t) z_b(t)}{z_{b0} v_{T0}} (1-\chi)^{n-1/2} \frac{\Gamma(n)}{\Gamma(n+1/2)}, & \chi \le 1, \\ 0, & \chi > 1 \, . \end{cases}$$

  - $n = 1$ and $\lambda \sim 1 - Z^2$,the distribution function $f \sim \sqrt{1-\chi}$ when $\chi \le 1$.
  - $n = 1/2$ and $\lambda \sim \sqrt{1 - Z^2}$, f is a flat-top function of χ.
  - $n < 1/2$, the distribution function diverges near $\chi = 1$.

Density Inversion Theorem

⇨ Another family of self-similar line density profiles

$$\lambda(t,z) = \lambda_b(t) h(Z^2) \; = \begin{cases} \lambda_b(t)(1 - Z^{2n}), & Z \le 1, \\ 0, & Z > 1 \, . \end{cases} .$$

$$f(\chi) = \begin{cases} -\frac{1}{\pi} \frac{\lambda_b(t) z_b(t)}{z_{b0} v_{T0}} \left[\sqrt{\pi} n \chi^{2n-1/2} \frac{\Gamma(1/2-2n)}{\Gamma(1-2n)} \right. \\ \left. + \frac{4n}{4n-1} F(\frac{1}{2}, \frac{1}{2} - 2n; \frac{3}{2} - 2n; \chi) \right] , \quad \chi \le 1, \\ 0, \; \chi > 1 \, . \end{cases}$$

⇨ $F(\frac{1}{2}, \frac{1}{2} - 2n; \frac{3}{2} - 2n; \chi)$ —hypergeometric function.

⇨ $2n \gg 1 \longrightarrow$ arbitrarily flat line density profiles.

Example: Pulse Shaping with Compression

- For the case of a beam being shaped but not compressed, $\alpha = 1$ and $V(\xi = 1) = 0$. When $\alpha > 1$, the beam is simultaneously being shaped and compressed, and $V(\xi = 1) < 0$.

- Initial pulse shape $\Lambda(z) = 1 - z^{15}$ and final pulse shape $\Lambda_T(z) = (135/32)(1 - 9z^2)$ are plotted in (a). The initial velocity $V(z)$ is plotted in (b).

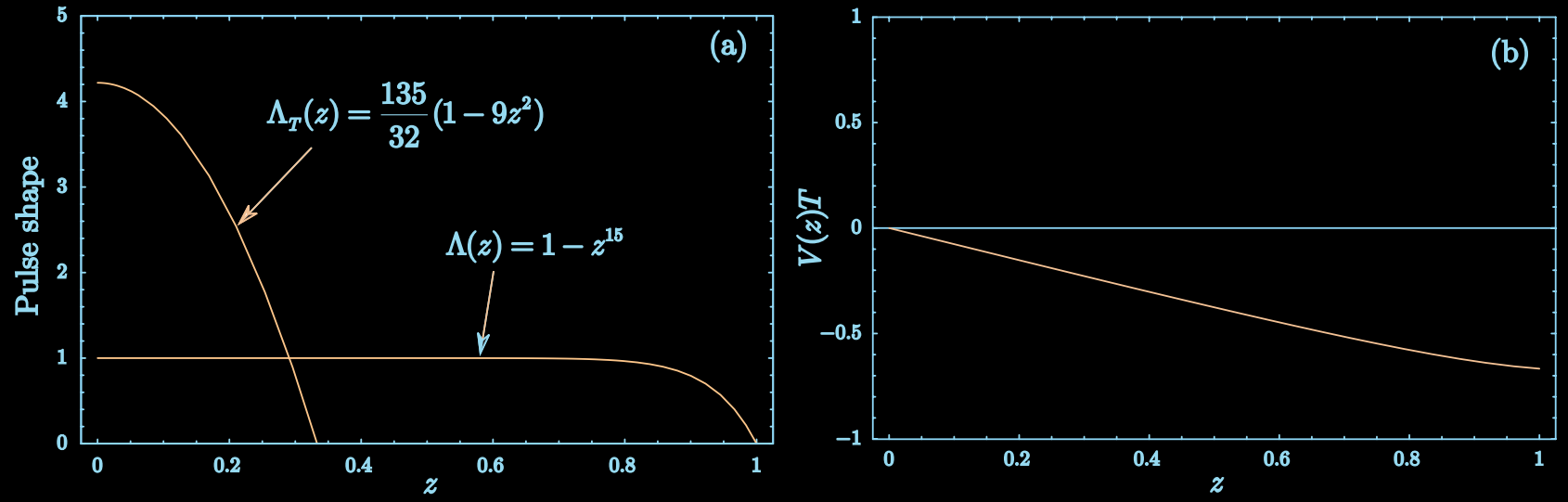

Correction for Deviation from the Symmetry

- To focus entire beam pulse onto the same focal, the self-similar symmetry condition need to be satisfied.
- Self-similar drift compression scheme satisfies the symmetry condition for the line density.
- It is difficult to guarantee the symmetry condition for the transverse emittance due to the complex dynamical behavior.
  - Longitudinal compression
  - Non-periodic transverse focusing lattice and final focus magnets.
- However, in most heavy ion fusion systems, the transverse emittance is small.
- The deviation from the self-similar symmetry condition due to the transverse emittance can be treated as a perturbation.
- Deliberately impose another perturbation to the system to cancel out the perturbation due to the un-symmetric transverse emittance.

Time-Dependent Lattice for Entire Pulse

- However, the emittance in general is small but not negligible, and does not scale with the perveance.
- In fact, during adiabatic drift compression, the emittance scales with the beam size, i.e., $\varepsilon_x \propto a$ and $\varepsilon_y \propto b$.
- Self-similar symmetry condition can't be satisfied.
- Vary the strength of four magnets in the very beginning of the drift compression for different value of z such that the self-similar symmetry holds at $s = s_{ff}$.
- Numerically, the necessary variation of the strength of the magnets is found by a 4D root-searching algorithm.
- A small perturbation in the strength of the magnets introduces a small envelope mismatch in such a way that the self-similar symmetry is satisfied at $s = s_{ff}$.

Transverse Dynamics for Central Slice

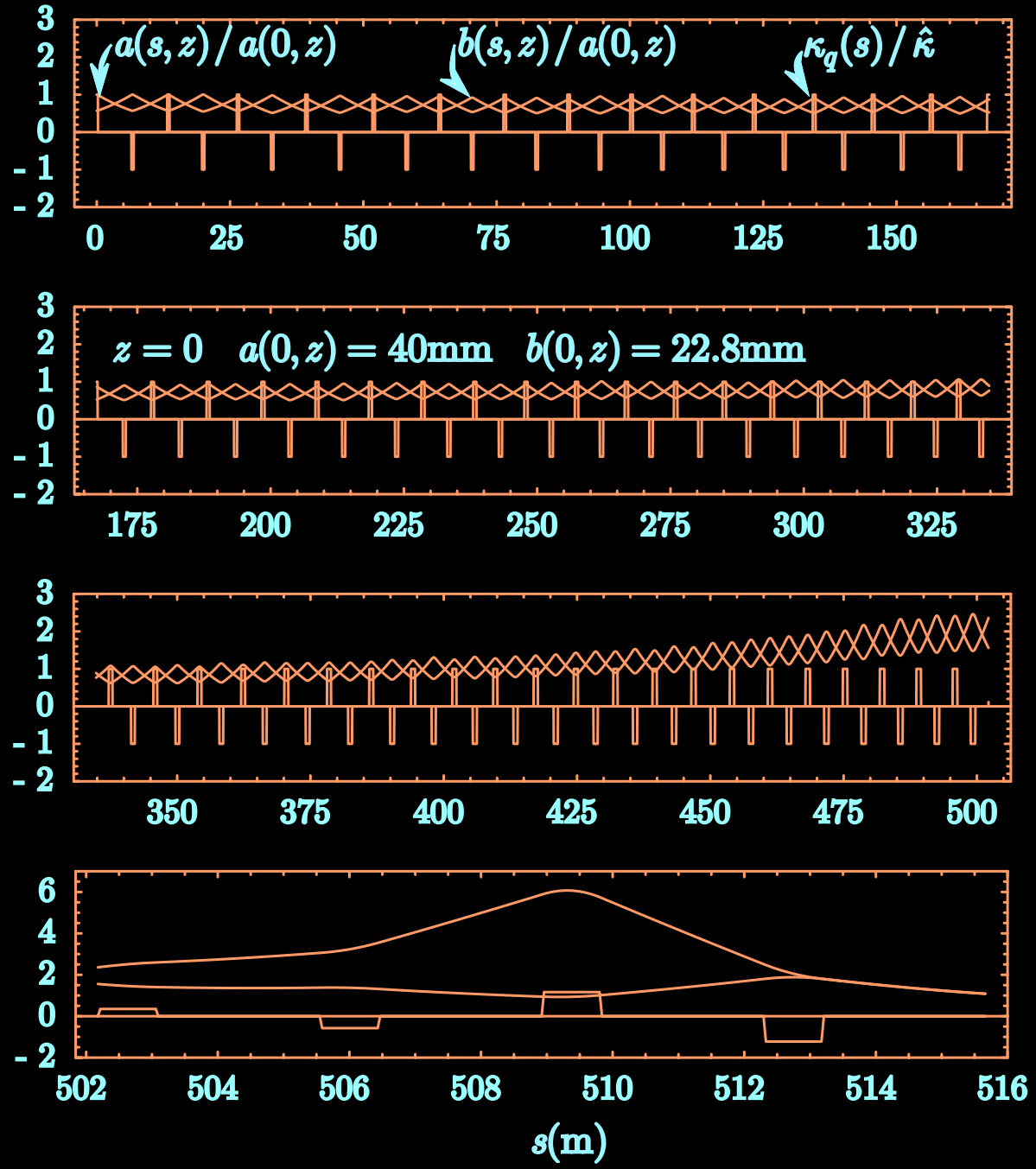

Envelope dynamics for the $z/z_b(s) = 0.968$.

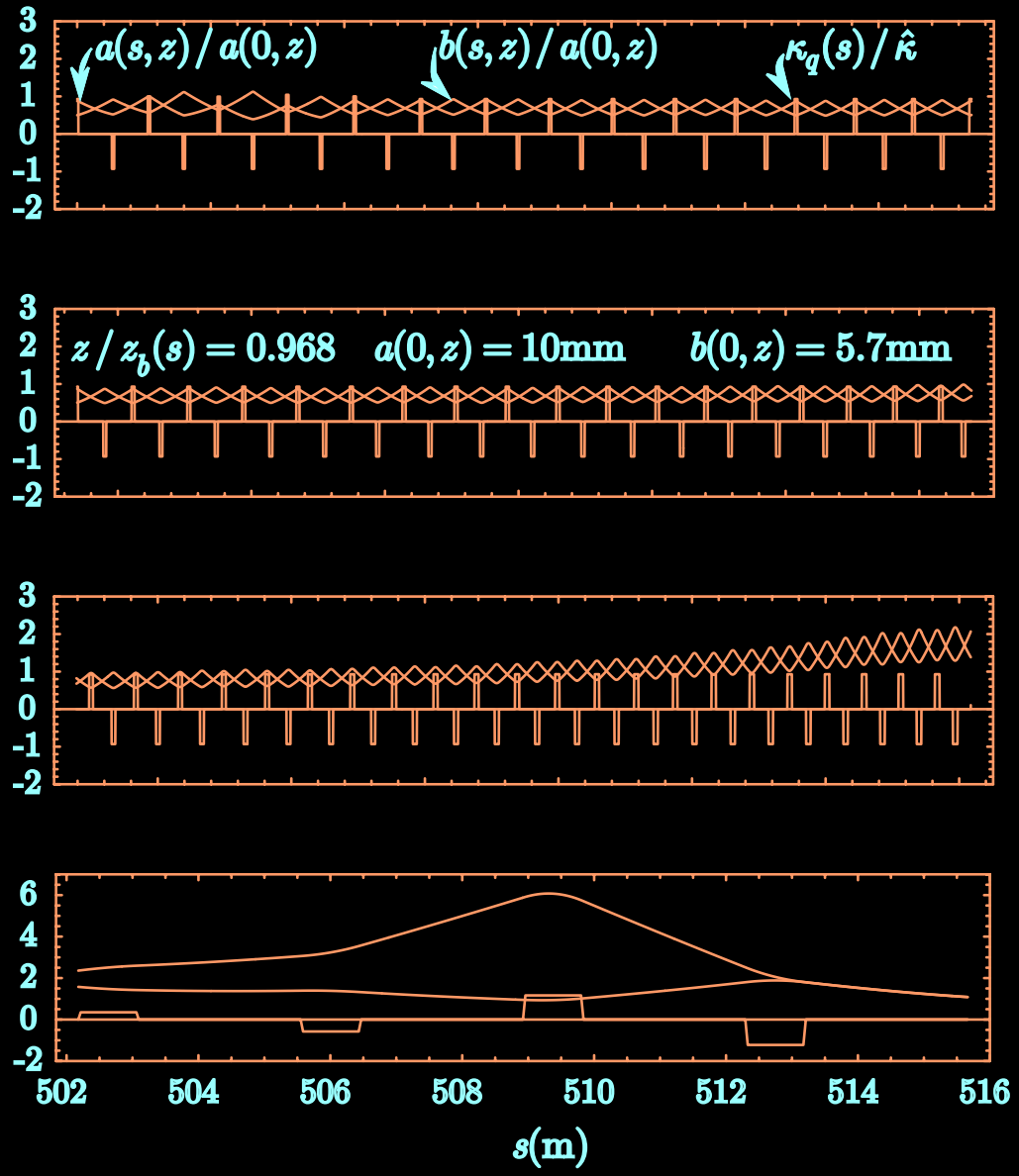

Time-Dependent Lattice for Entire Pulse

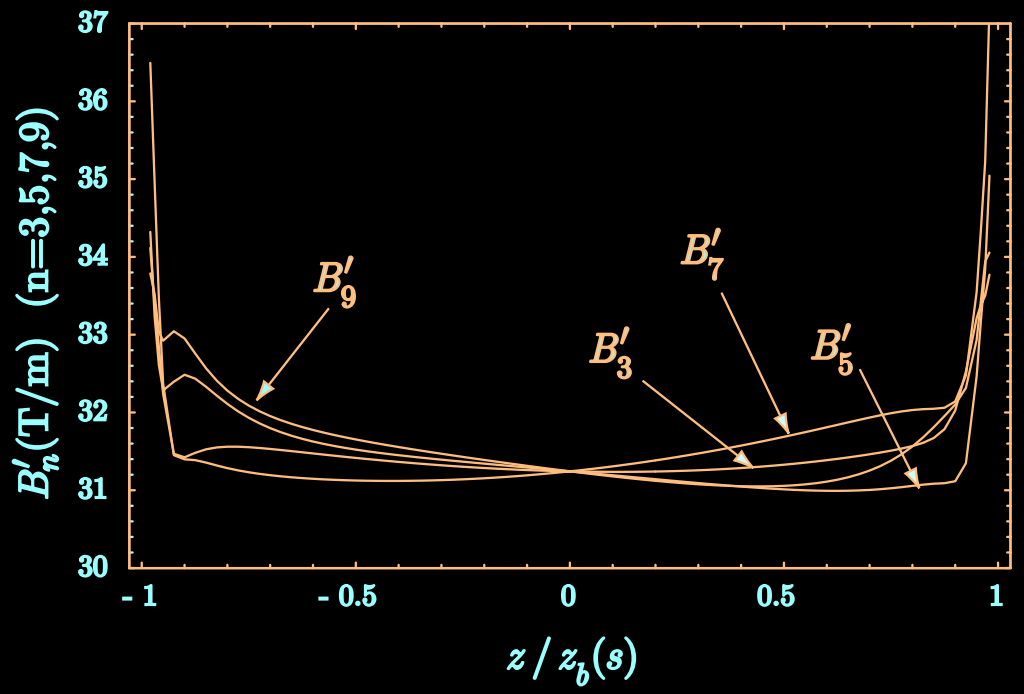

Figure 1: Strengths of the 3rd, 5th, 7th, and 9th magnets as functions of $z/z_b(s)$.

System of Equations

$$\frac{\partial n_e}{\partial t} + \nabla \bullet \left(n_e \vec{V}_e \right) = 0,$$

$$\frac{\partial \vec{p}_e}{\partial t} + (\vec{V}_e \bullet \nabla)\vec{p}_e = -\frac{e}{m}(\vec{E} + \frac{1}{c}\vec{V}_e \times \vec{B}),$$

$$\nabla \times \vec{B} = \frac{4\pi e}{c}\left(Z_b n_b V_{bz} - n_e V_{ez} \right) + \frac{1}{c}\frac{\partial \vec{E}}{\partial t},$$

$$\nabla \times \vec{E} = -\frac{1}{c}\frac{\partial \vec{B}}{\partial t}.$$

Steady- State Results (current flow)

Beam propagates in the y-direction, beam half length l_b=15 c/ω_p ; beam radius r_b =1.5 c/ω_p ; beam density n_b is equal to the background plasma density n_p; beam velocity V_b=$c/2$.

Shown are the normalized electron density n_e/n_p and the vector fields for the current.

FOR MORE INFO...

http://hifnews.lbl.gov/hifweb08.html

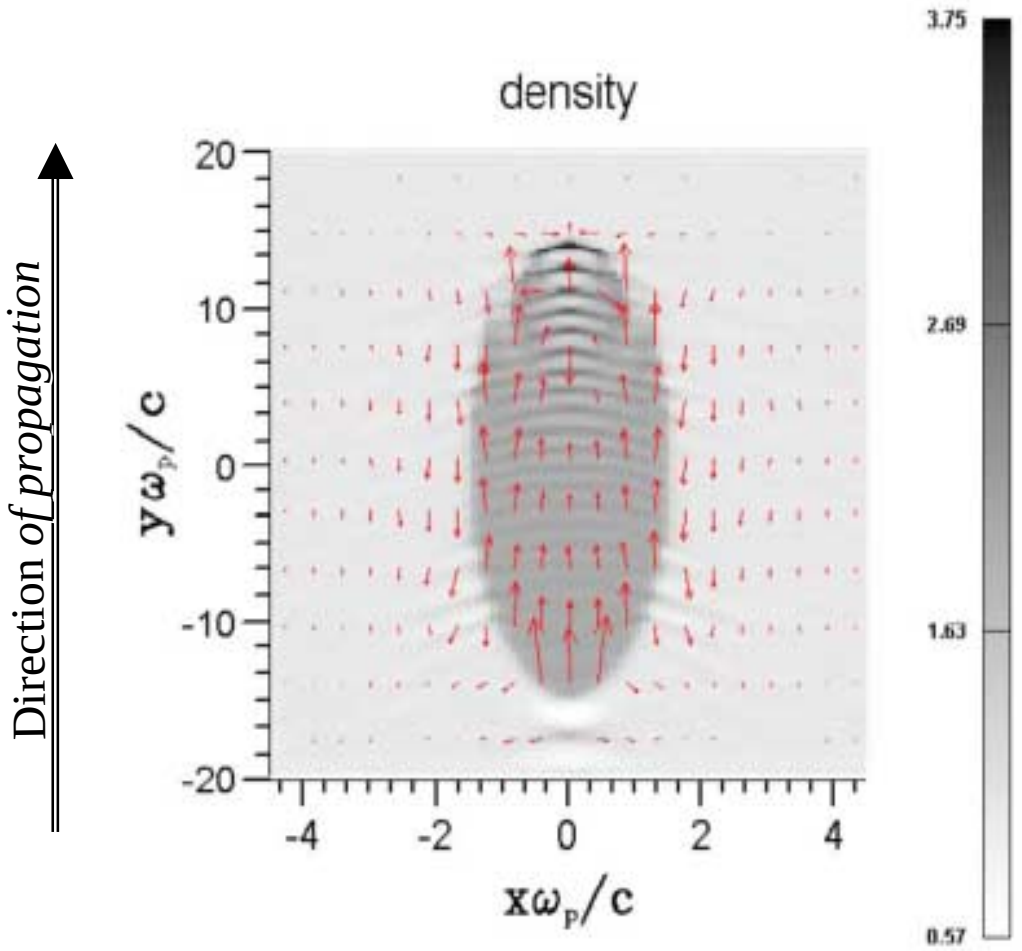

Analytic theory of chamber transport: excitation of plasma waves by beam depends on bunch length

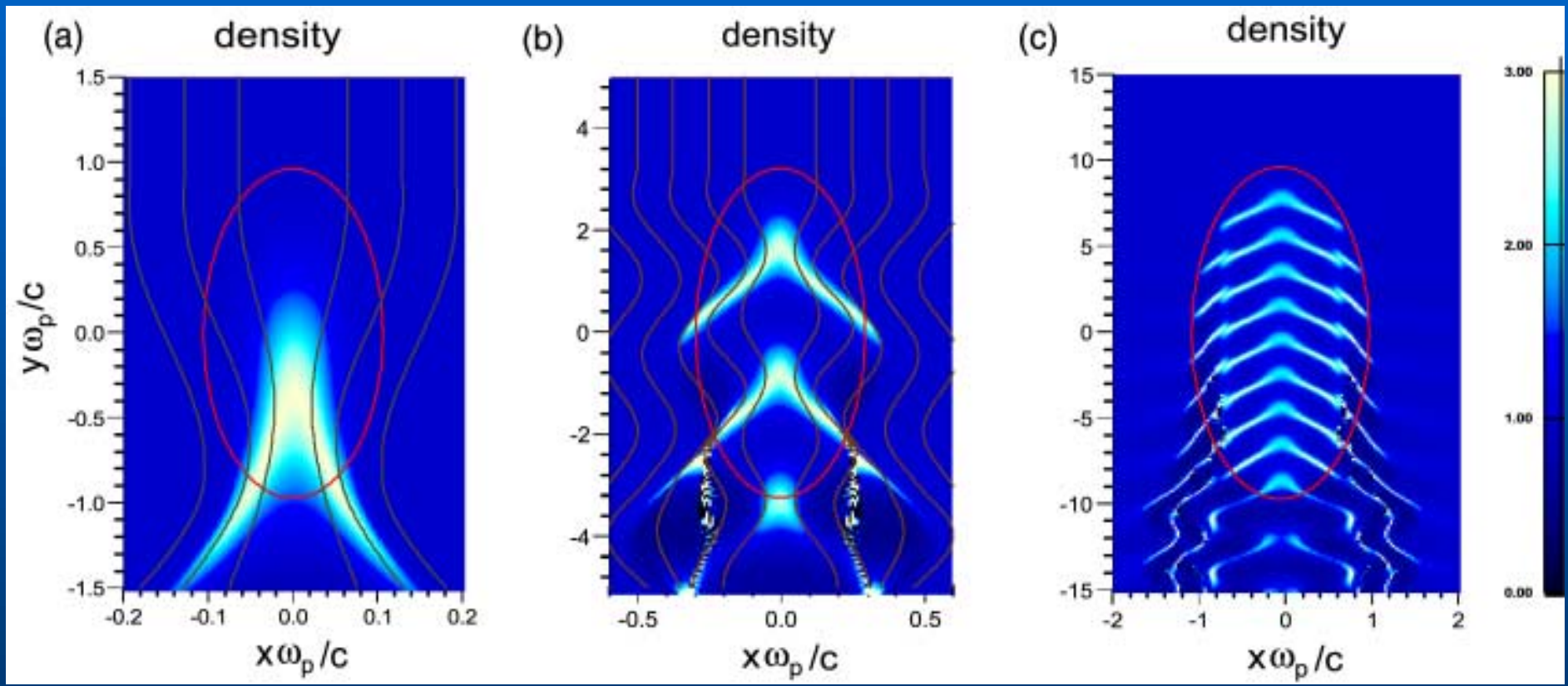

β_b=0.5, l_b/r_b =10, n_b/n_p=0.5 a) $l_b = 2V_b/\omega_p$, b) $l_b = 6V_b/\omega_p$, c) $l_b = 20V_b/\omega_p$.
Red line: ion beam size, brown lines: electron trajectory in beam frame

Ion Beam Interaction with Background Plasma

Candidate Instabilities

- Resistive Hose
- Multispecies Weibel
- Multispecies Two-Stream

Resistive Hose Instability

Assumptions

- Step-function density profile.
- Transverse electromagnetic dipole-mode perturbations

$$\delta\mathbf{E}^T = \delta E_z \hat{\mathbf{e}}_z \ , \quad \delta\mathbf{B}^T = \delta B_r \hat{\mathbf{e}}_r + \delta B_\theta \hat{\mathbf{e}}_\theta$$

- Charge neutralizing plasma background

$$\sum_{j=b,e,i} n_j^0(r) e_j = 0$$

- Partial current neutralization

$$J_{zp} = -f_m(\hat{n}_b e_b \beta_b c)$$

Resistive Hose Instability

Dipole-mode perturbations with

$$\delta E_z(\mathbf{x},t) = \delta\hat{E}_z(r)\,\exp[i(\theta - \Omega z/V_b - \omega\tau)]$$

where $\Omega = \omega - k_z V_b$.

Dispersion relation is given by

$$\frac{\hat{\omega}_{pb}^2\beta_b^2}{\Omega^2 - \omega_\beta^2} = -\kappa_p r_b \frac{J_1'(\kappa_p r_b)}{J_1(\kappa_p r_b)} - \frac{r_w^2 + r_b^2}{r_w^2 - r_b^2}\ ,$$

where

$$\omega_\beta^2 = \frac{1}{2}\hat{\omega}_{pb}^2\beta_b^2(1 - f_m)\ ,$$

$$\kappa_p^2(\omega) r_b^2 = \frac{8i\omega\tau_d}{(1 - i\omega/\nu_c)}\ .$$

Resistive Hose Instability

Illustrative Example

- 1 kA, 2.5 GeV cesium beam.
- $\widehat{n}_b = 3.4 \times 10^{11} cm^{-3}$; beam radius $r_b = 1cm$.
- Zero plasma return current ($f_m = 0$).
- For $T_e = 1$ eV and $\widehat{n}_e = 10^{12} cm^{-3}$ we obtain:

$$\sigma_p = 3 \times 10^{12} s^{-1} (\text{conductivity})$$

$$\tau_d = \frac{\pi \sigma_p r_b^2}{2c^2} = 5 \times 10^{-9} s (\text{magnetic decay time})$$

- Resulting growth rate is

$$Im\Omega = 0.13\omega_\beta$$

where $\omega_\beta = 9.2 \times 10^6 s^{-1}$.

Growth Rate Reduction Mechanisms

- Proximity of a conducting wall.
  - Increasing $g = \left(1 - \frac{r_b^2}{r_w^2}\right)^{-1}$.
- Increasing the value of $|\omega|/\nu_c$.
- Decreasing the value of fractional current neutralization f_m.
  - Stabilizing influence of B_θ.
- Rounded beam density profile.
  - Reduces number of resonant beam particles.
- Increase electron temperature.
  - Higher plasma conductivity.

Resistive Hose Instability

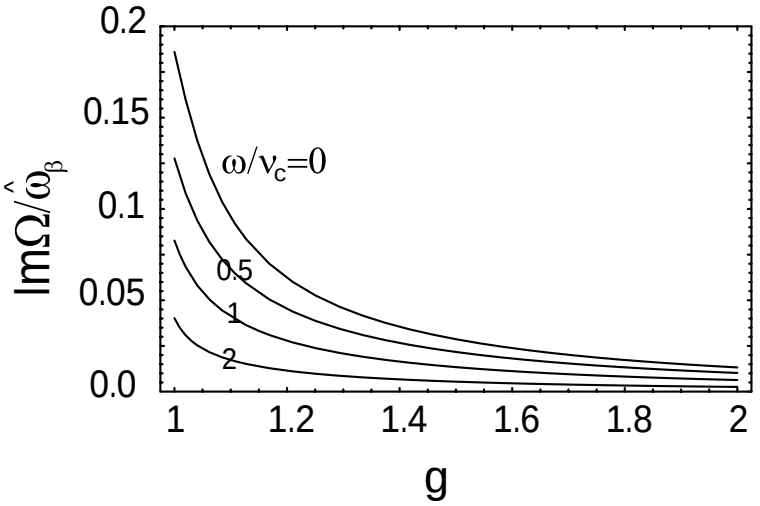

Instability growth rate is reduced by increasing values of $|\omega|/\nu_c$ and by the proximity of a conducting wall, i.e., increasing $g = \left(1 - \frac{r_b^2}{r_w^2}\right)^{-1}$.

Beam modeling and simulation play important roles in the research projects at the US Heavy Ion Fusion Virtual National Laboratory.

- Algorithm and code development.
- Large-scale parallelization and visualization.
- Simulation and experimental observation.
- Simulation and theoretical predication.

Numerical modeling poses formidable challenges

- Challenges in accelerator modeling include
  - ✓ efficient but detailed description of applied fields
  - ✓ time-dependent space-charge limited emission in 3-D
  - ✓ 10^7 - 10^8 particles, ~ 10^5 steps, > 100 cells in x and y, 1000's in z
  - ✓ multi-beam effects
- Challenges in chamber modeling include
  - ✓ complex physics models
  - ✓ dense plasma; need implicit hybrid model
  - ✓ large grid, esp. for multi-beam runs; 10^7 - 10^8 particles
- Comparisons with experiment can be difficult
  - ✓ quadrupole focusing $\Rightarrow$ sensitivity to diagnostic locations
  - ✓ diagnostics are typically projections of phase space

Time scales in driver and chamber span a wide range

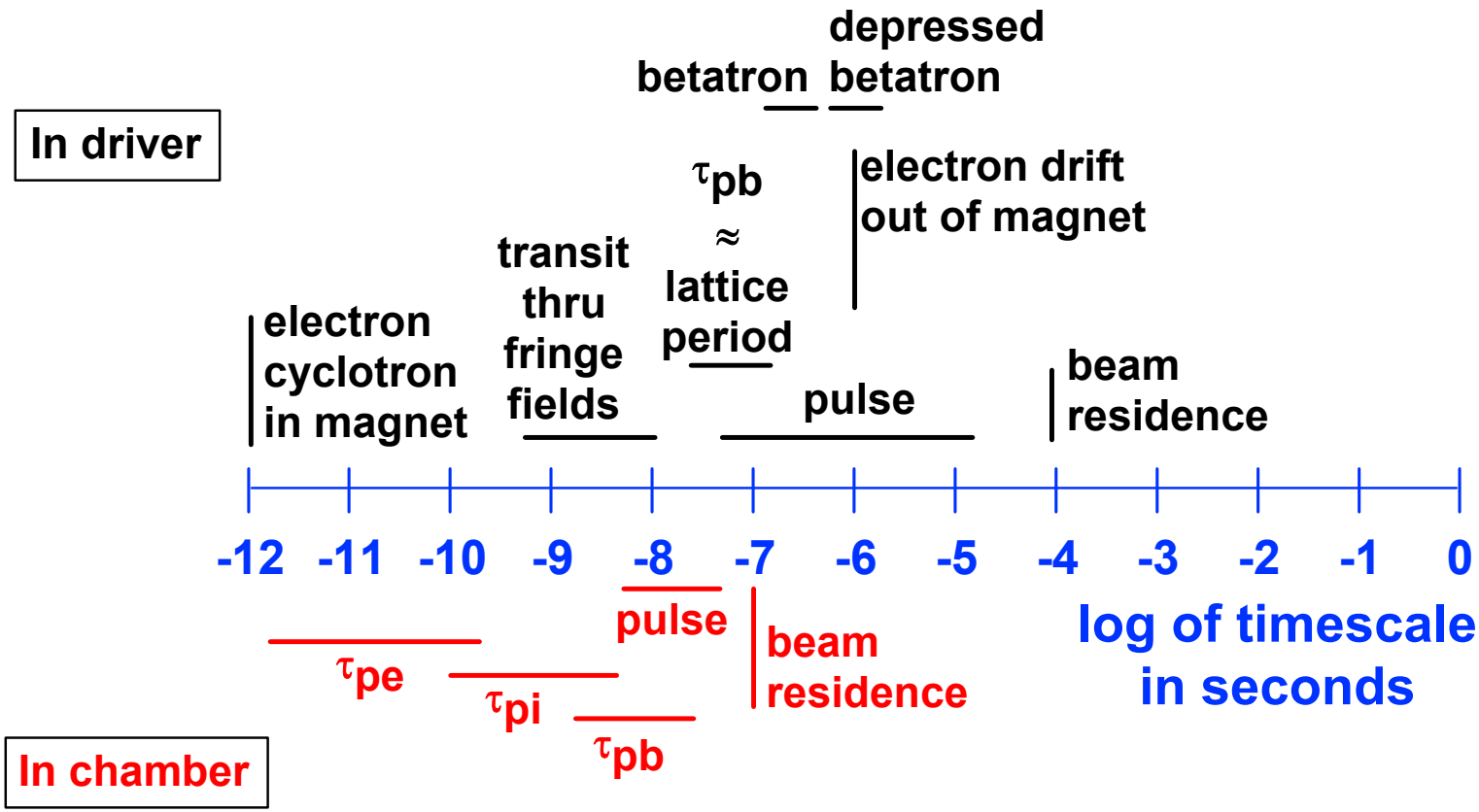

Scale lengths range from electron gyroradius in magnet ~.01 mm to $l_{D,beam}$ ~ 1 mm, to beam radius ~ cm, to machine length ~ km's

HIF Computer Codes

The HIF Virtual National Laboratory has developed a suite of computer codes for modeling beam injection, acceleration, transport, and focusing in induction accelerators and transport in a fusion chamber. Our goal is an integrated, detailed, and benchmarked source-to-target beam simulation capability.

WARP An electrostatic code with envelope, PIC, and Vlasov models to examine beam injection and transport.

LSP An implicit electromagnetic PIC code with a particle-fluid electron model for modeling high-density plasmas.

BEST A nonlinear perturbative PIC code for studying questions of beam stability and halo formation.

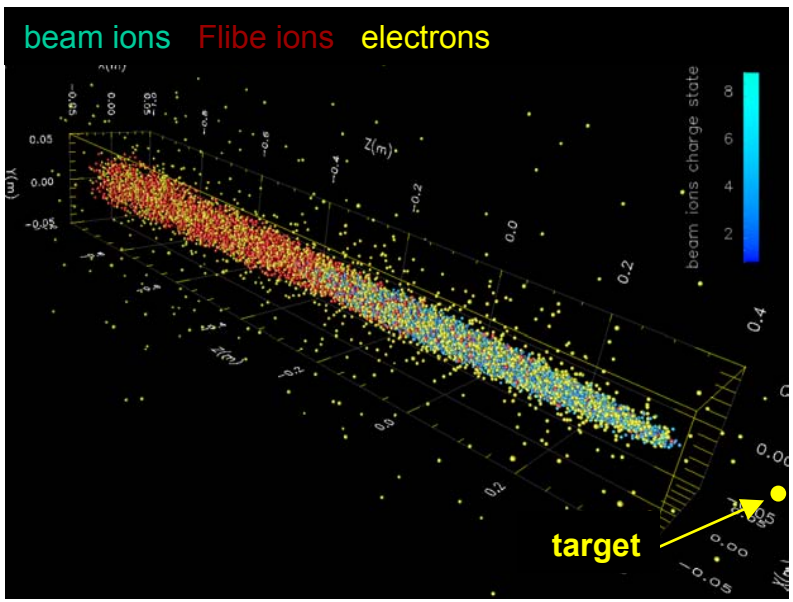

beam propagation in chamber

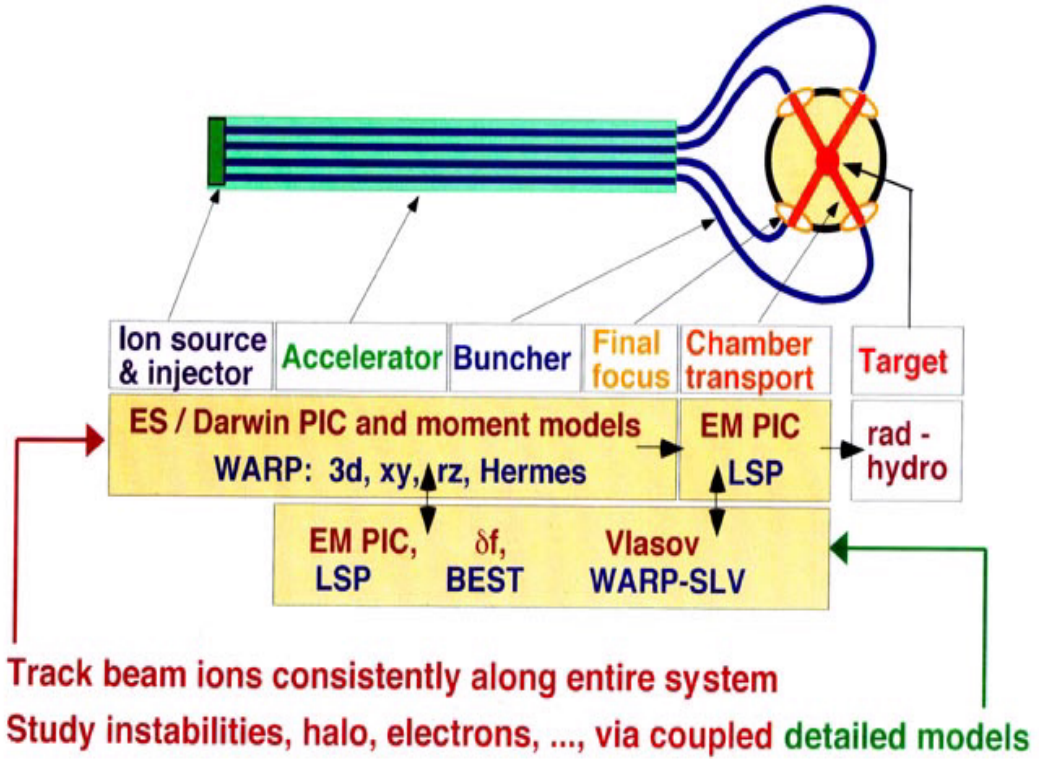

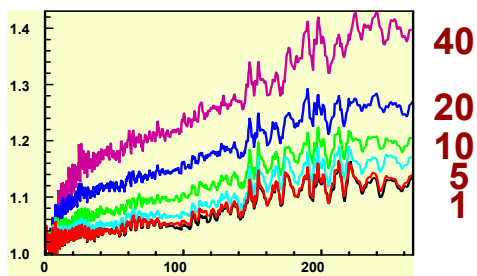

emittance growth and beam steering

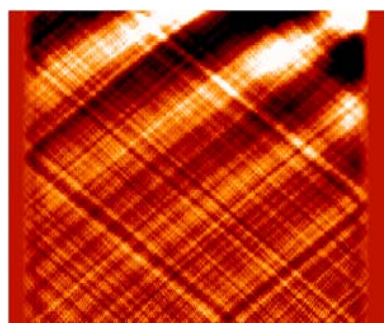

waves on beam

HIF is at the forefront of beam and plasma simulation

The novel feature of BEST is its use of the so-called δf method, in which equations for deviations from a known, unperturbed, but in general time-dependent beam equilibrium are advanced. When perturbed quantities are sufficiently small, this approach has several advantages over conventional PIC codes.

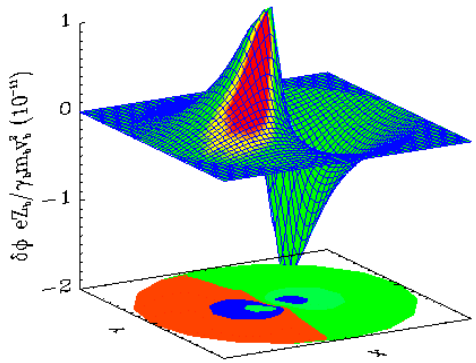

3-D δf code BEST shows structure of two-stream mode

4-D SLV simulation

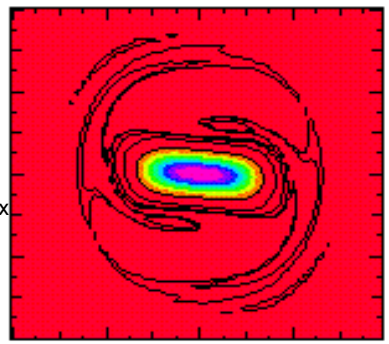

Semi-Lagrangian Vlasov beam simulations advance the phase-space density on a multi-dimensional grid. Such methods, currently under development, offer the promise of a large dynamic range. In contrast with discrete-particle methods, Vlasov methods represent the low-density parts of phase space with fidelity similar to that of the main beam, thus facilitating study of the physics of beam halos.

In collaboration with NERSC, we are pioneering the use of Adaptive Mesh Refinement (AMR) in 3-D beam and plasma particle simulations. The AMR technique, originally developed in fluid mechanics, provides a "numerical zoom" capability that gives high resolution only where it is needed, allowing a major reduction in the size and cost of computations. Sample calculations show a fourfold reduction in computational cost with nearly identical results.

Source simulation with AMR

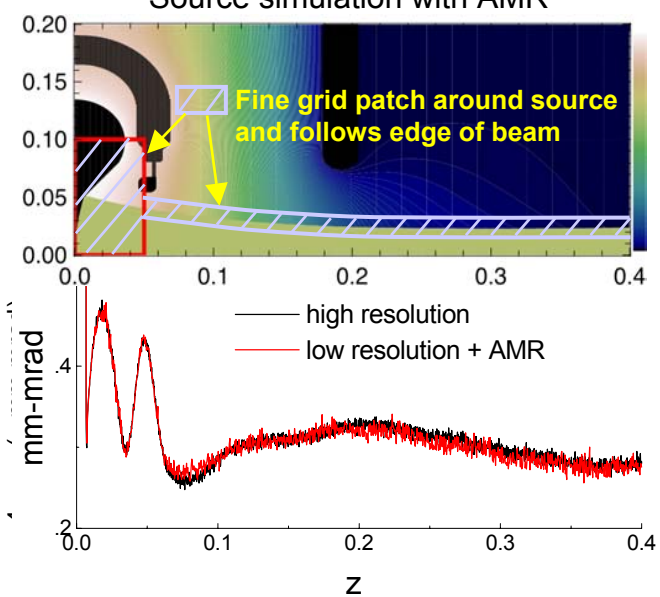

Prototype AMR implemented in WARPrz

- **Higher speedup obtained with a "true" dynamic AMR implementation**

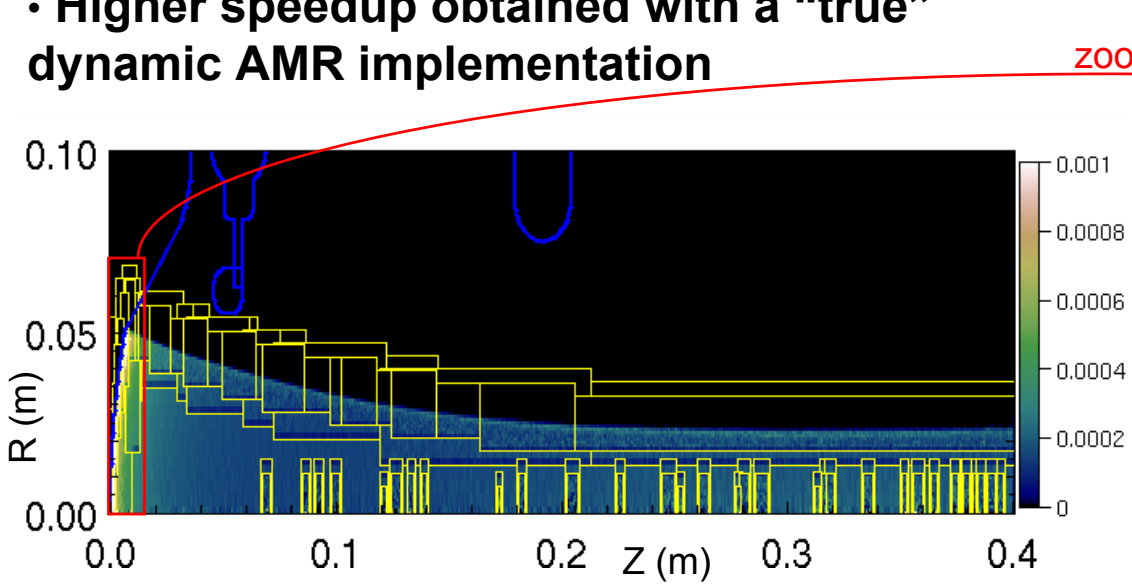

zoom

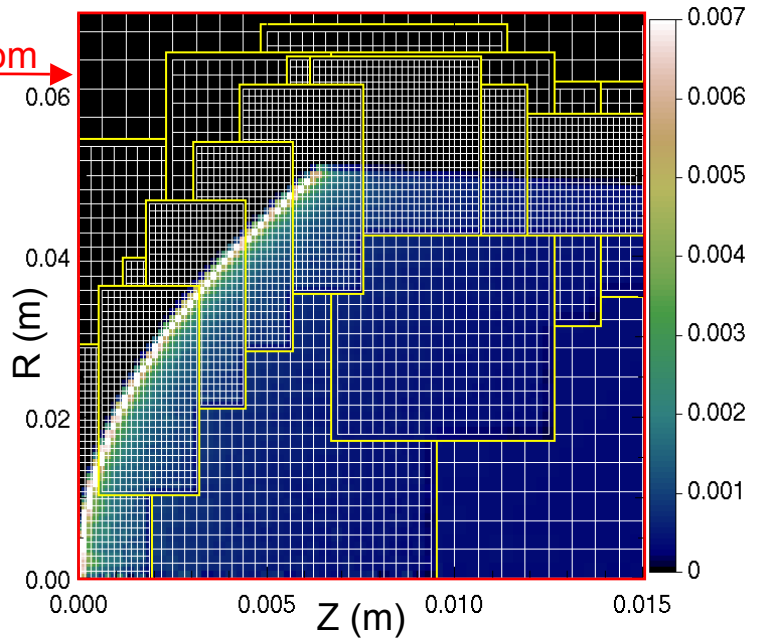

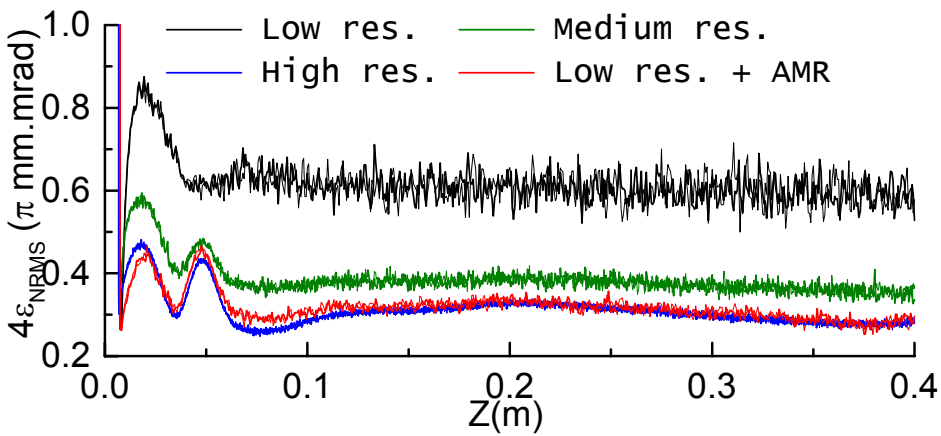

In this case: speedup ~ 11.3

WARP simulations model STS-500 experiments using 10-cm-diameter K^+ alumino-silicate source

Rise time

Current at Faraday cup

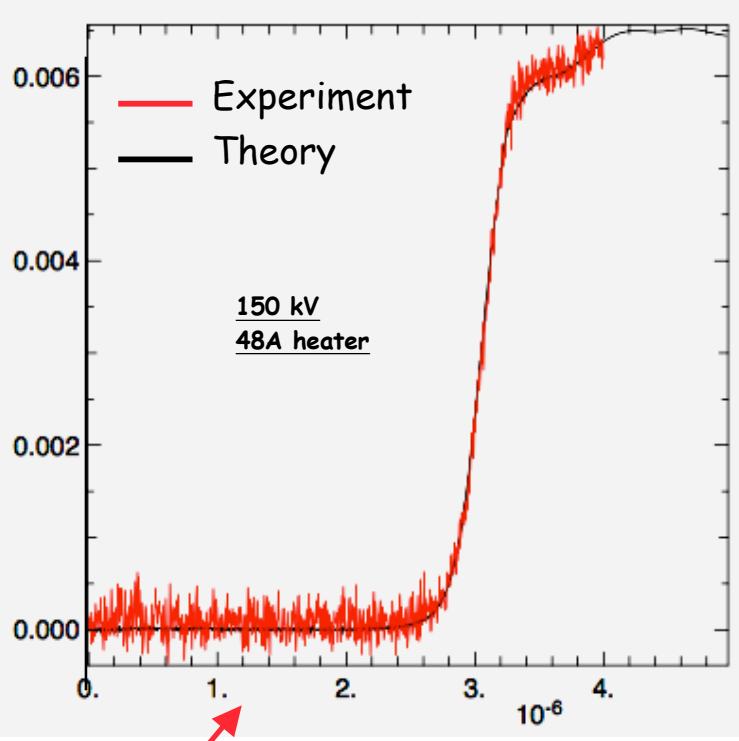

Result depends critically on Mesh Refinement

Phase Space at End of Diode

Warp simulations

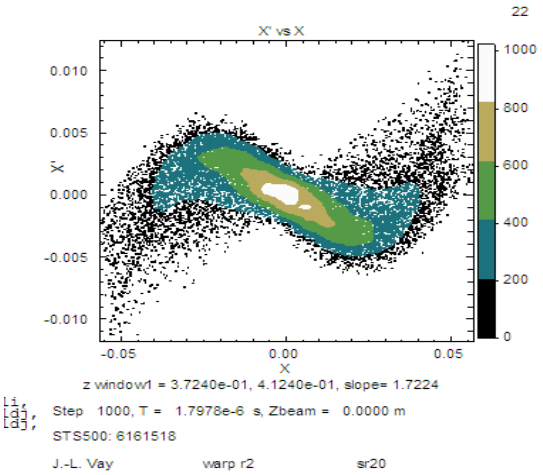

Experimental results

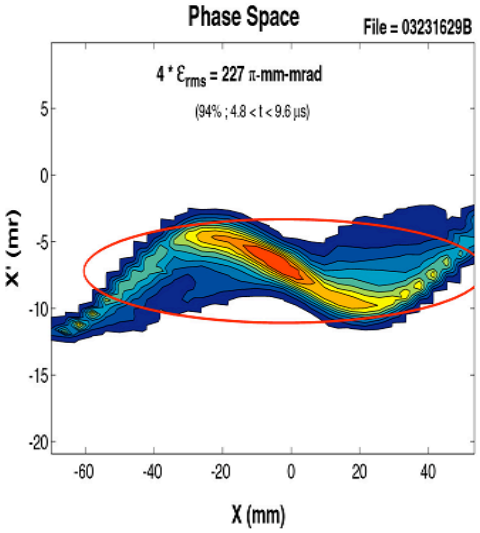

(simulations by I. Haber, J-L. Vay, D. P. Grote)

3D WARP simulation of HCX shows beam head scrapping

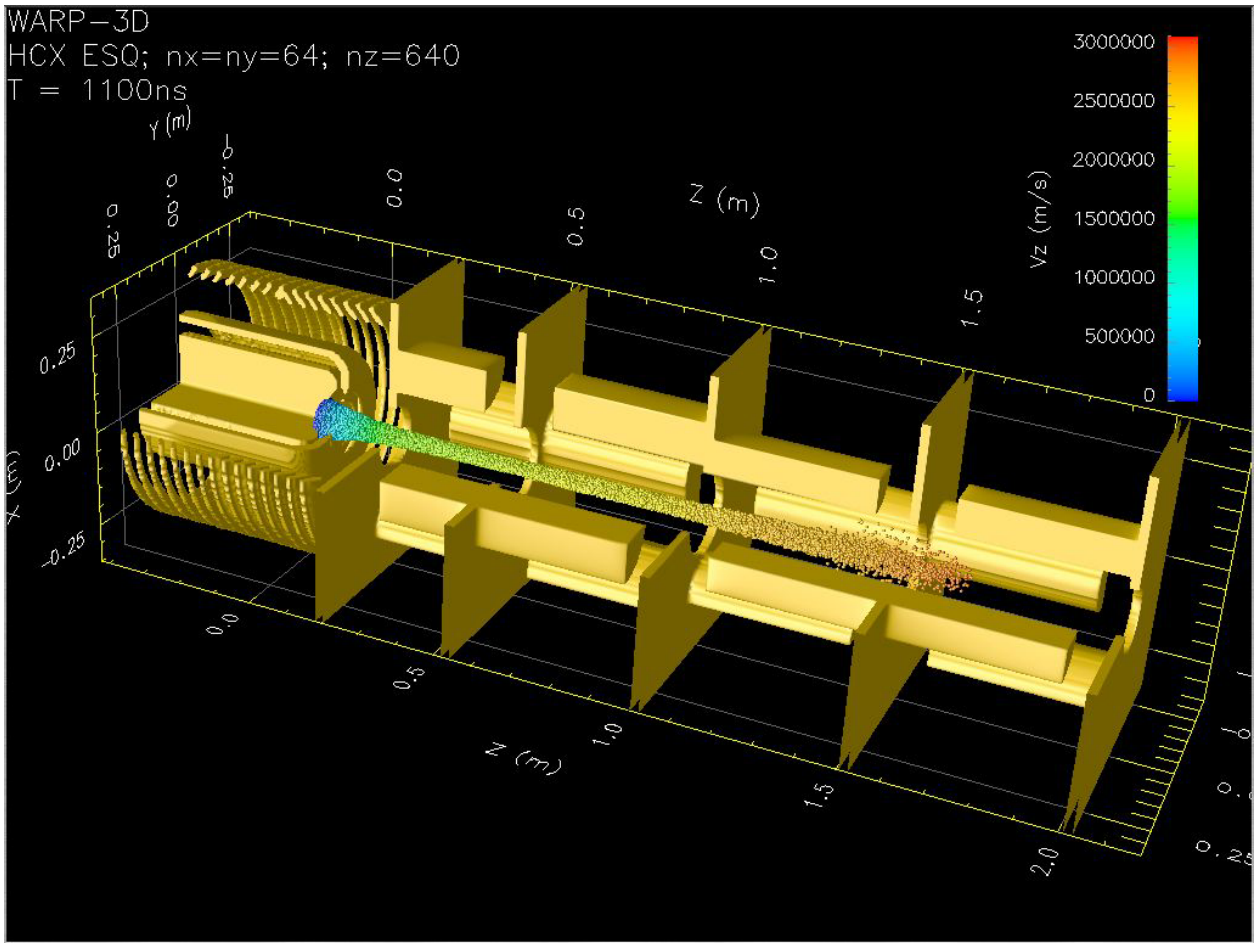

Rise-time τ = 800 ns
beam head particle loss < 0.1%

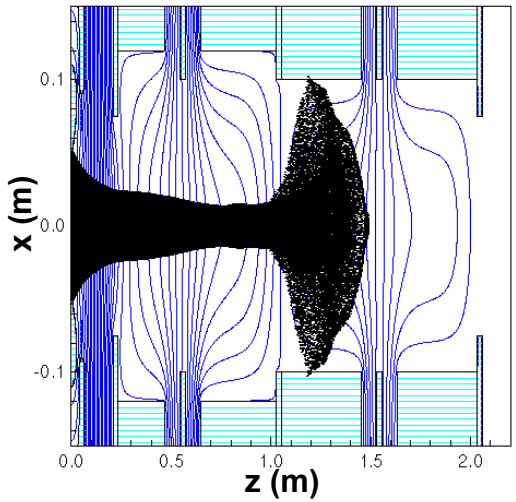

Rise-time τ = 400 ns
zero beam head particle loss

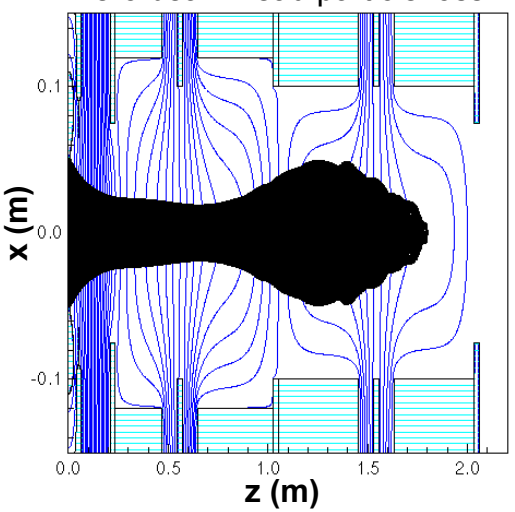

- **Can we get even cleaner head with faster rise-time?**
- **Optimum?**

WARP simulations of the UMER electron gun reproduce some features of the observed velocity space

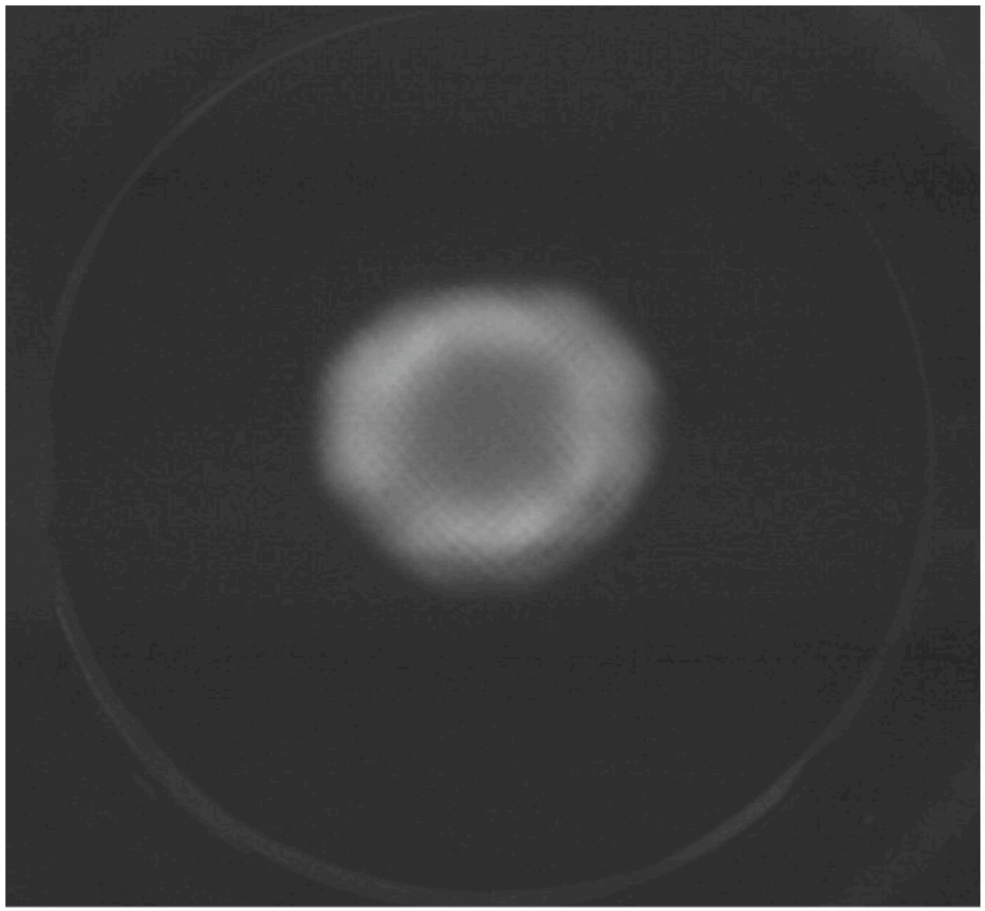

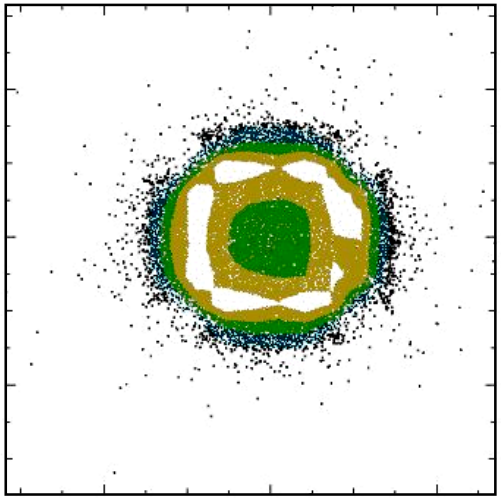

Beam velocity distribution emerging from the gun, measured as a phosphor screen image of the beam after passage through a small hole

(simulations by I. Haber / R. Kishek)

Harris Instability in Intense One-Component Beams

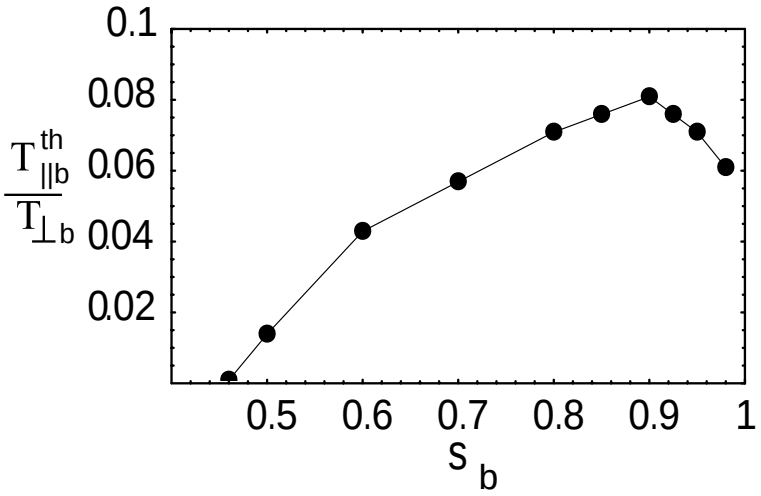

Longitudinal threshold temperature $T^{th}_{\|b}$ normalized to the transverse temperature $T_{\perp b}$ for the onset of instability plotted versus normalized beam intensity $s_b = \hat{\omega}^2_{pb}/2\omega^2_f$.

Harris Instability in Intense One-Component Beams

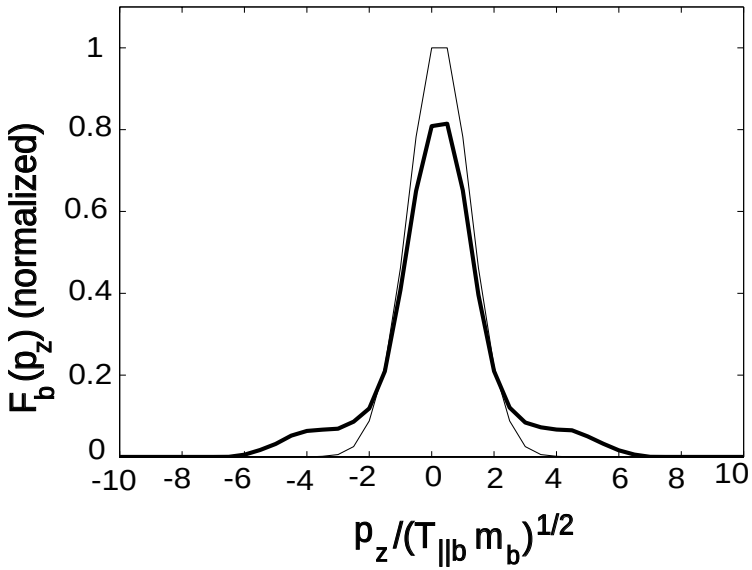

Plot of average longitudinal momentum distribution $F_b(p_z, t)$ at time $t = 0$ (thin line) and $t = 150\omega_f^{-1}$ (thick line), for normalized beam intensity $s_b = 0.8$ and $T_{\|b}/T_{\perp b} = 0.02$.

Harris Instability in Intense One-Component Beams

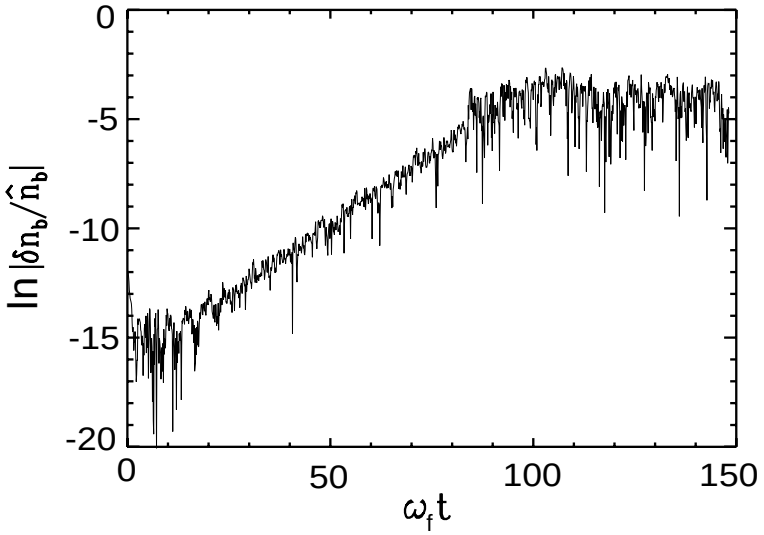

Time history of the normalized density perturbation $\delta n_{\max}/\hat{n}_b$ for $s_b = 0.8$ and $T_{\|b}/T_b = 0.02$ at fixed axial position z and radius $r = 0.3r_b$.

Electron-Ion Two-Stream (Electron Cloud) Instability

BEST simulations have been carried out for 3D perturbations about distribution functions ($j = b, e$)

$$f_j^0(r, \mathbf{p}) = \frac{\widehat{n}_j}{2\pi\gamma_j m_j T_{\perp j}} \exp\Big(- \frac{H_{\perp j}}{T_{\perp j}}\Big) G_j(p_z)$$

For the beam ions, take $G_b(p_z)$ to be a drifting Maxwellian centered at $p_z = \gamma_b m_b V_b$. For the background electrons take $G_e(p_z)$ to be a Maxwellian centered at $p_z = 0$.

Illustrative Parameters

Linearized δF simulations for 2.5 GeV cesium ion beam with

$$f = \frac{\widehat{n}_e}{\widehat{n}_b} = 0.1 \ , \quad \frac{T_{b\perp}}{\gamma_b m_b V_b^2} = 1.1 \times 10^{-6} \ , \quad \frac{T_{e\perp}}{\gamma_b m_b V_b^2} = 2.47 \times 10^{-6}$$

Electron-Ion Two-Stream (Electron Cloud) Instability

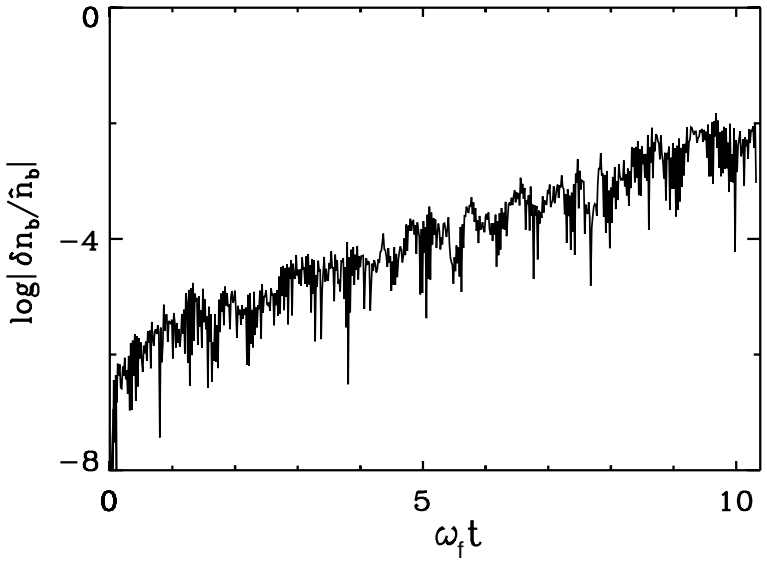

Time history of perturbed density $\delta n_b/\tilde{n}_b$ at a fixed spatial location. After an initial transition period, the $m = 1$ dipole-mode perturbation grows exponentially.

Electron-Ion Two-Stream (Electron Cloud) Instability

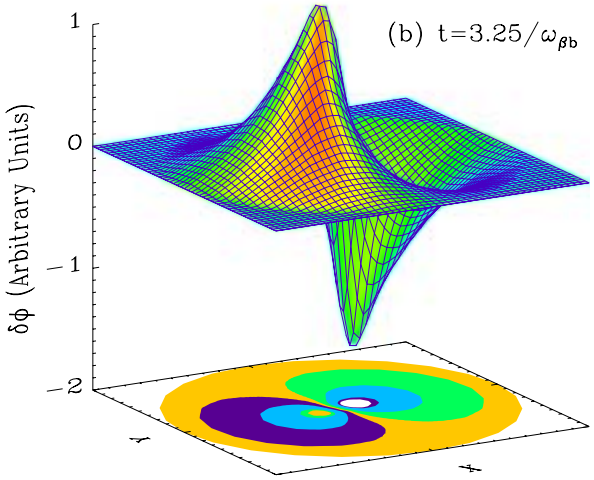

The $x-y$ projection (at fixed value of z) of the perturbed electrostatic potential $\delta\phi(x, y, t)$ for the ion-electron two-stream instability growing from a small initial perturbation, shown at $\omega_f t = 3.25$.

Electron-Ion Two-Stream (Electron Cloud) Instability

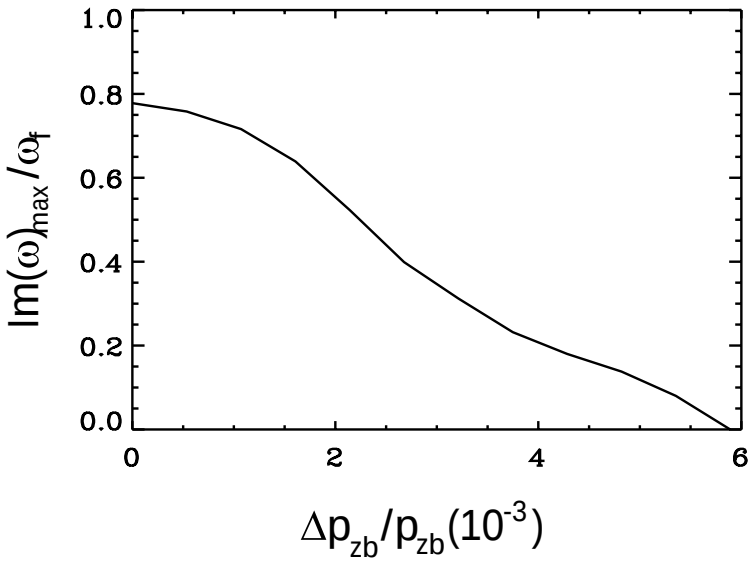

The maximum linear growth rate $(Im\omega)_{\max}$ of the ion-electron two-stream instability decreases as the longitudinal momentum spread of the beam ions increases.

Drift compression with pulse shaping

phase space at stagnation shows good end control

- **about 12% of charge at stagnation is in ends**
- **large velocity swings during shaping introduce nonuniformity**
- **high final emittance may result from this nonuniformity**

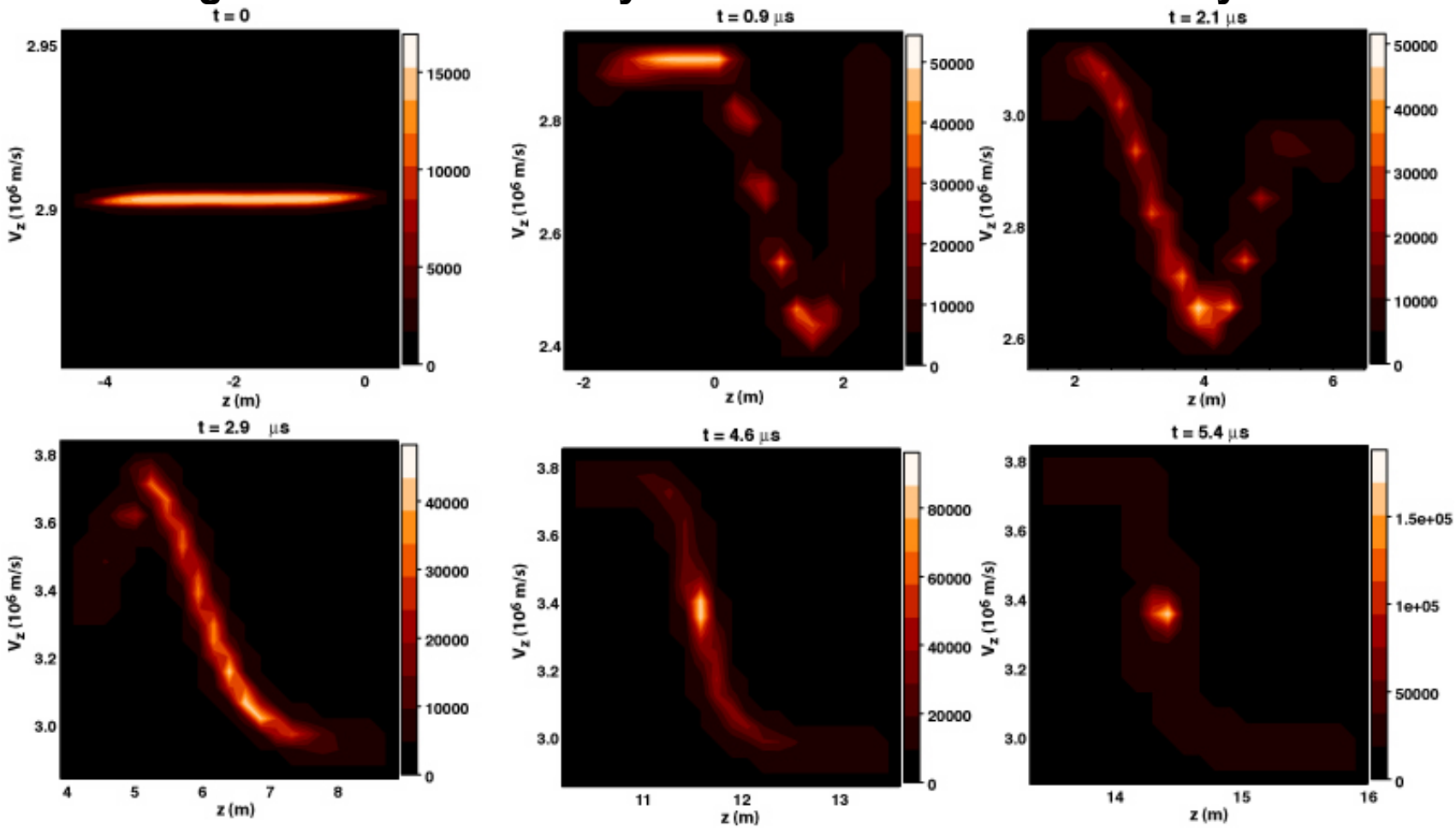

Preliminary LSP simulations for a modular IFE driver show neutralized compression and focusing in a 100-m plasma column

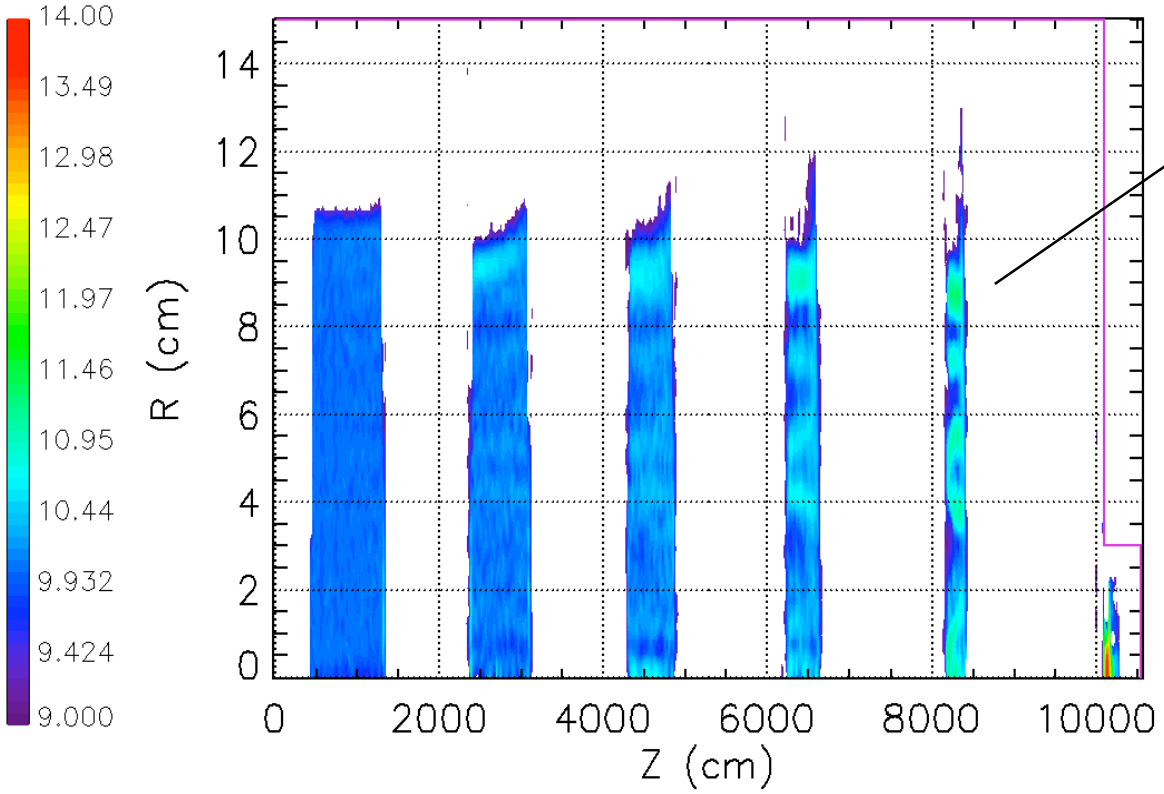

Run shows filamentation, but 92% of beam still falls within the 5 mm spot needed for a hybrid distributed radiator target

Ne^{+} beam
Pulse energy: 140 kJ
Energy ramp: 200 - 240 MeV
Current: 3 140 kA
Beam radius: 10 cm < 5 mm
Pulse duration: 210 5 ns

Other LSP simulations are playing a major role in scoping out the "NDCX" experiments to begin in the near future

(Simulations by D.Welch & D. Rose)

LSP is used to examine in some depth NDC instability and transport issues

NTX* MEASUREMENT

6-mA, 254-keV, 2-cm K^+ beam, with L = 1m

With plasma plug

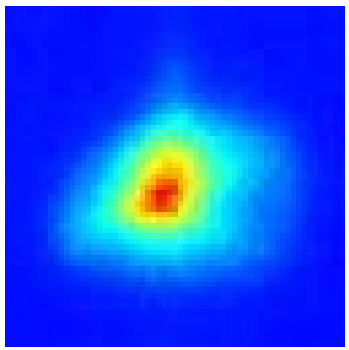

With plasma plug and RF Plasma

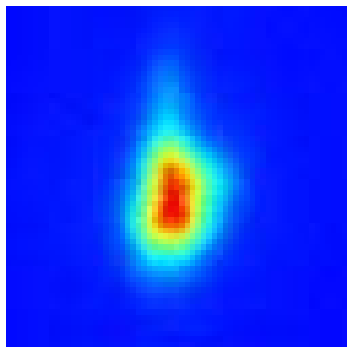

100% neutralization

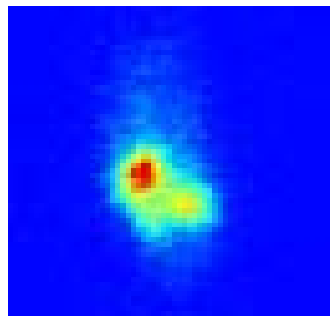

LSP SIMULATIONS

With plasma plug

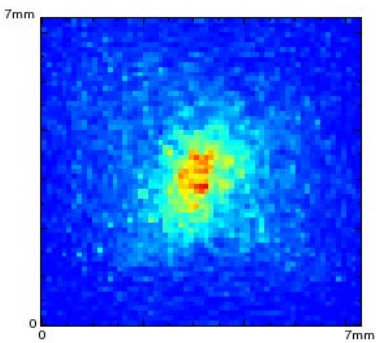

With plasma plug and RF Plasma

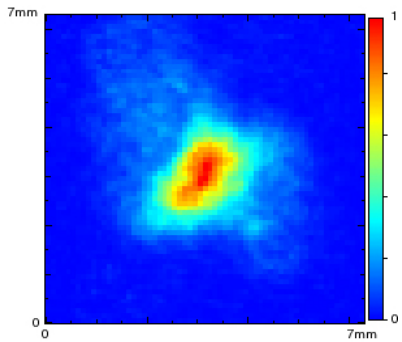

100% neutralization

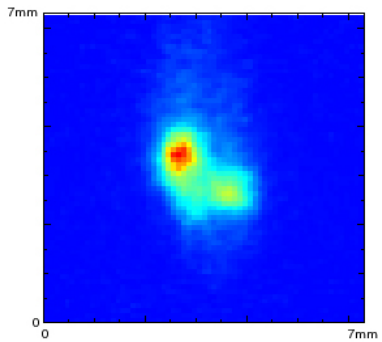

LSP is being benchmarked in plasma neutralization experiments on NTX

*See Th.I-5 P. Roy